Maximal symmetry transition paths for reconstructive phase transitions

2007 J. Phys.: Condens. Matter 19 275203

(http://iopscience.iop.org/0953-8984/19/27/275203)

IOP PUBLISHING JOURNAL OF PHYSICS: CONDENSED MATTER

J. Phys.: Condens. Matter **19** (2007) 275203 (16pp) doi:10.1088/0953-8984/19/27/275203

Maximal symmetry transition paths for reconstructive phase transitions

C Capillas, J M Perez-Mato and M I Aroyo

Departamento de Fisica de la Materia Condensada, Universidad del País Vasco, Apartado 644, (48080) Bilbao, Spain

E-mail: cesar.capillas@ehu.es

Received 15 March 2007, in final form 28 March 2007
Published 1 June 2007
Online at stacks.iop.org/JPhysCM/19/275203

Abstract

An essential part of the description of a reconstructive phase transition consists in the determination of the so-called transition path, which defines the possible atomic displacements and lattice strains that occur during the transformation. We present a systematic procedure for the determination of possible transition paths in phase transitions with no group–subgroup relation between their phases. It is assumed that the transformation involves, at least locally, an intermediate state described by a common subgroup of the symmetry groups of the two end phases. The possible mappings between the end structures are restricted by symmetry constraints following from the occupied atomic orbits, and tolerances for lattice strains and atomic displacements. The concept of maximal symmetry transition paths is used for the classification of the different symmetry allowed transition paths. The application of the procedure is illustrated by the determination of maximal symmetry transition paths for the transformations from wurtzite to rocksalt, zincblende to rocksalt and rocksalt to caesium chloride structure types.

The prediction and characterization of the atomistic mechanisms that govern first order phase transitions with no group–subgroup relation between their phases has become of great interest in the last few years, in particular from the viewpoint of the possibilities now offered by the DFT *ab initio* methods. Typical subjects of these studies are the so-called reconstructive phase transitions, which constitute the most widespread type of structural phase transitions in nature. Reconstructive phase transitions may lead to huge *reorganizations* of the atomic positions with a change, in general, in the coordination numbers of the atoms. Another example of transitions with no group–subgroup relation between their phases, but not implying large atomic reorganizations, is given by the transformations between ferroelectric phases with different orientations of the polarization which are driven either by temperature or field. Reconstructive phase transitions and in general, first order phase transitions in crystals are

in principle governed by nucleation processes, but this is not in contradiction with the fact that on a local basis these transformations may involve diffusionless cooperative displacements of the atoms, which result in transient intermediate local configurations that can be given an approximate crystalline character. Molecular dynamical simulations have indeed evidenced these transient intermediate configurations on the interfaces separating the two phases [1]. Making abstraction of this property, one can consider these transient configurations as a homogeneous crystalline state that links in a continuous form the two end phases with higher symmetries. We can talk then of a *transition path*. A transition path can be defined as the set of atomic displacements and lattice strains that can make the system transit in a continuous way from one phase to the other. In the simplest case, one assumes that a minimal set of symmetry breaks or gains takes place during the transformation, so that the intermediate state has the same symmetry all along the transformation, and is given by a common subgroup of the space groups of the two end phases. This intermediate state defines a possible *trajectory* or *transition path* in the configuration space of the system that continuously maps the two end phases. A transition path specifies the atomic displacements and lattice strains that are supposed to take place at a local level during the transformation. In general, for two given phases, the number of possible transition paths is infinite, because the number of common subgroups is infinite. To limit the problem and restrict it to the most probable mechanisms, one can limit the cell multiplication of the intermediate subgroup. For a given cell multiplication, it is possible to obtain a finite set of common subgroups.

A symmetry analysis cannot predict the energetically most favourable transition path. This would require to explore the *energy landscape* and, in particular, the energy barriers that separate two stable phases, establishing the most favourable transition paths in the configuration space [2, 3]. However, a complete exploration of the configuration space is not possible, and it is necessary to make a previous selection of the most favourable subspaces. The symmetry criteria are essential for a logical [4] and systematic selection of these subspaces [5]. The knowledge of the most favourable transition paths is also of considerable interest for some particular applications. For example, the comprehension of the symmetry relations between the two stable phases may result in simple phenomenological models that permit to determine the topology of its phase diagram [6]. In addition, the transition path determines the relative orientation of the two phases and their eventual domain structure. And finally, in some cases the different intermediate states are candidates for new stable phases, particularly at high pressure, in the same or analogous systems [7].

One of the first attempts for the description of reconstructive phase transitions, in terms of an initial limited break of symmetry and a later symmetry gain, is given by Cahn [8] in the study of the fcc $\rightarrow$ bcc transformation in Fe. Later, Dmitriev and Toledano [6] developed a modified Landau formalism based on the definition of an order parameter periodical with the displacements, that has been successfully applied to the study of considerable transitions. The method for the determination of possible transition paths used by Sowa combines symmetry considerations and geometrical models based on deformation of heterogeneous sphere packings (see e.g. [9]). Stokes and Hatch have applied an approach based on symmetry and structural criteria combined with energetical calculations to several cases, among them, the transformations between CsCl and NaCl [10], or zincblende to NaCl [11] structure types.

In the following sections, we present a method for a systematic determination of possible transition paths in terms of (i) their symmetry relations, which include the analysis of the group–subgroup relations and the splittings of the occupied Wyckoff positions in the common subgroup, and (ii) the structural conditions related to tolerable values for the lattice strains and atomic displacements. A useful classification scheme for the symmetry possible transition paths is achieved by introducing the concept of maximal symmetry transition paths.

The application of the procedure is illustrated by several examples of reconstructive phase transitions: the transformations between wurtzite and rocksalt, zincblende and rocksalt, and rocksalt and CsCl-structure types.

1. Symmetry conditions on transitions paths

Consider two crystalline structures S_1 and S_2 with space group symmetries $\mathcal{G}_1$ and $\mathcal{G}_2$, which are not group–subgroup related. The structures are described by the lattice parameters, the positions of the atoms, and the number of formula units Z_1 and Z_2 per conventional unit cell. A transformation between the two structures can then be described as a three-step process, starting with an initial limited symmetry break $\mathcal{G}_1 \rightarrow \mathcal{H}_1$, with $\mathcal{H}_1 \simeq \mathcal{H}$, where a hypothetical sublattice of the initial lattice is obtained with exactly the same lattice parameters or a multiple of them, and having lost some symmetry operations of $\mathcal{G}_1$. Next, the lattice of the subgroup $\mathcal{H}_1$ is distorted by an affine transformation without an additional change of symmetry $\mathcal{H}_1 \rightarrow \mathcal{H}_2$, with $\mathcal{H}_1 \simeq \mathcal{H}_2$, accompanied by atomic displacements that are compatible with the common subgroup symmetry. Finally, a symmetry gain $\mathcal{H}_2 \rightarrow \mathcal{G}_2$ takes place, where new symmetry operations not belonging to $\mathcal{G}_1$ appear. The three-step factorization of the symmetry change $\mathcal{G}_1 \rightarrow \mathcal{G}_2$ allows the application of symmetry restrictions to the group–subgroup pairs $\mathcal{G}_1 > \mathcal{H}_1$ and $\mathcal{G}_2 > \mathcal{H}_2$, and quantitative structural criteria for the change $\mathcal{H}_1 \rightarrow \mathcal{H}_2$. Note that a full description of a transition path requires not only the definition of the pair of subgroups $(\mathcal{H}_1, \mathcal{H}_2)$, but also the identification of atomic displacements that link pairwise the atomic positions in both phases.

1.1. Indices of a common subgroup of two space groups

The symmetry reductions $\mathcal{H}_1 < \mathcal{G}_1$ and $\mathcal{H}_2 < \mathcal{G}_2$ are characterized by the indices $i_1 = |\mathcal{G}_1|/|\mathcal{H}|$ and $i_2 = |\mathcal{G}_2|/|\mathcal{H}|$. According to Hermann's theorem [12], these indices of $\mathcal{H}$ in $\mathcal{G}_1$ and $\mathcal{G}_2$ can be uniquely factorized into *translationengleiche* and *klassengleiche* parts:

$$i_q = i_q^t \cdot i_q^k \qquad \text{where } i_q^t = \frac{|\mathcal{P}_q|}{|\mathcal{P}_\mathcal{H}|} \qquad \text{for } q = 1, 2 \tag{1}$$

being $\mathcal{P}_q$ and $\mathcal{P}_\mathcal{H}$ the point groups of the space groups $\mathcal{G}_q$ and $\mathcal{H}$. The indices i_q^t are related to the reduction of the point group symmetry during the symmetry break $\mathcal{G}_q \rightarrow \mathcal{H}_q$, and i_q^k corresponds to the multiplication of the primitive unit cell in the subgroup. It is obvious that the number of formula units per primitive unit cell for the structures S_1 and S_2 must be the same when described in their subgroups $\mathcal{H}_1$ and $\mathcal{H}_2$. This is forced by the assumed continuous transformation within the space group type $\mathcal{H}$ linking the two structures. This means that $Z_1 \cdot i_1^k/f_1 = Z_2 \cdot i_2^k/f_2$, where f_1 and f_2, are the corresponding centring factors[1]. Taking into account equation (1) this implies the following relation between the indices i_1 and i_2 of the two group–subgroup branches $\mathcal{G}_1 > \mathcal{H}_1$ and $\mathcal{G}_2 > \mathcal{H}_2$:

$$i_2 = i_1 \cdot \frac{Z_1}{Z_2} \cdot \frac{|\mathcal{P}_2|}{|\mathcal{P}_1|} \cdot \frac{f_2}{f_1}. \tag{2}$$

1.2. Common subgroups of two space groups

Once the common subgroup types and the corresponding indices are obtained, the next step in the symmetry analysis of the possible transition paths for the change $\mathcal{G}_1 \rightarrow \mathcal{G}_2$ consists

[1] The centring factor for a P-lattice is equal to 1, for I-, A-, B- or C-lattices is 2, for a R-lattice is 3, and for a F-lattice is equal to 4.

in the calculation of the subgroups for the two group–subgroup branches, the sets $\{\mathcal{H}_{1,r}, r = 1, \ldots, n\}$ with index i_1 in $\mathcal{G}_1$, and $\{\mathcal{H}_{2,s}, s = 1, \ldots, m\}$, with index i_2 in $\mathcal{G}_2$. The set of possible subgroups $\mathcal{H}_{1,r}$ and $\mathcal{H}_{2,s}$ are distributed in classes of conjugated subgroups with respect to $\mathcal{G}_1$ and $\mathcal{G}_2$, respectively. The subgroup $\mathcal{H}_{q,k}$ with $q = 1, 2$ is specified by a matrix-column pair $(\boldsymbol{P}, \boldsymbol{p})_{q,k}$ which determines the transformation between the conventional bases of $\mathcal{G}_q$ and $\mathcal{H}_{q,k}$. Each of the $n \cdot m$ pairs $(\mathcal{H}_{1,r}, \mathcal{H}_{2,s})$ and the corresponding transformation matrices, defines a possible symmetry for the transition path between $\mathcal{G}_1$ and $\mathcal{G}_2$.

It is important to take into consideration:

(i) In our treatment we specify $\mathcal{H}_{q,k}$ by the transformation matrix $(\boldsymbol{P}, \boldsymbol{p})_{q,k}$. However, one should note that the choice of $(\boldsymbol{P}, \boldsymbol{p})_{q,k}$ is not unique: its arbitrariness is determined by the normalizer of $\mathcal{H}$. In other words, two transformation matrices which differ by a matrix belonging to the normalizer of $\mathcal{H}$ correspond to the same subgroup, i.e. the same subset of elements of $\mathcal{G}_q$, and therefore define transition paths that are not distinguishable from purely symmetry criteria.

(ii) It is expected that physically distinguishable paths would result for subgroups that belong to different conjugacy classes with respect to $\mathcal{G}_1$, and with respect to $\mathcal{G}_2$. Different conjugacy classes of subgroups describe different low symmetry structures, while subgroups belonging to the same conjugacy class are related to different physically equivalent domain states.

1.3. Wyckoff position matching rule

During a symmetry break $\mathcal{G} \rightarrow \mathcal{H}$, atoms that are symmetrically equivalent under $\mathcal{G}$, i.e. belong to the same orbit, may become non-equivalent under $\mathcal{H}$ (the orbit splits) and/or their site symmetry is reduced. This behaviour is the same for all orbits belonging to a Wyckoff position, and it is known as Wyckoff position splitting [13, 14].

Consider the two experimentally observed structures S_1 and S_2 which are specified by the coordinates of the occupied atomic orbits. Further restrictions on the possible transition paths for the transformation $\mathcal{G}_1 \rightarrow \mathcal{G}_2$ are due to the matching of the Wyckoff position splitting schemes for the group–subgroup pairs $\mathcal{G}_1 > \mathcal{H}_1$ and $\mathcal{G}_2 > \mathcal{H}_2$ as stressed on [15]: it is necessary by continuity[2] that the occupied orbits in $\mathcal{H}_1$ for a given atom type in S_1 coincide with the occupied orbits in $\mathcal{H}_2$ of the same atom type in S_2.

To apply this Wyckoff position matching condition it is necessary to take into account the fact that different Wyckoff positions of a space group may permute under isomorphic mappings of the space group onto itself, i.e. under the normalizer of the group. This could lead to some *fictitious* non-matching between the Wyckoff position splitting schemes due to the arbitrariness of the transformation matrix. In order to overcome this difficulty, the requirement for the strict coincidence of the Wyckoff position splitting schemes should be relaxed to include the matching of the splitting schemes up to Wyckoff positions belonging to the same Wyckoff set.[3]

1.4. Maximal symmetry transition paths

From the above discussion, the symmetry conditions for a transition path can be summarized as follows:

[2] No order–disorder mechanisms are envisaged.

[3] The sets of all those Wyckoff positions of a space group that are permuted under the normalizer of the group form the so-called Wyckoff sets. Tables of the Wyckoff sets for all space groups are published in [16].

(i) The intermediate state in a transition path is characterized by a pair of common isomorphic subgroups $(\mathcal{H}_1, \mathcal{H}_2)$ such that $\mathcal{G}_1 > \mathcal{H}_1$ and $\mathcal{G}_2 > \mathcal{H}_2$ with indices i_1 and i_2 which should be related by equation (2).

(ii) The occupied Wyckoff positions in $\mathcal{H}_1$ and $\mathcal{H}_2$ for each atom type should be the same or equivalent under the normalizer $\mathcal{N}(\mathcal{H})$.

Let us note that a pair of subgroups $(\mathcal{K}_1, \mathcal{K}_2)$ of $(\mathcal{H}_1, \mathcal{H}_2)$, such that $\mathcal{K}_1 < \mathcal{H}_1 < \mathcal{G}_1$ and $\mathcal{K}_2 < \mathcal{H}_2 < \mathcal{G}_2$ fulfils automatically these symmetry conditions if they are satisfied by $\mathcal{H}_1$ and $\mathcal{H}_2$. The use of symmetry criteria cannot predict the most favourable transition path from an energetical viewpoint. But it allows to classify the possible paths, and to hierarchize them. Those of greater symmetry will be in general more probable. The free energy is always extremal (minimal or maximal) with respect to a symmetry break. As the energy maps are usually smooth, in many cases the *valleys* of the energy correspond to configurations of greater symmetry, where the minimum is being forced by symmetry. For that reason it is important to introduce the concept of transition paths of maximal symmetry. We say that a transition path $(\mathcal{H}_1, \mathcal{H}_2)$ has *maximal symmetry* if there exists no pair of intermediate subgroups $(\mathcal{Z}_1, \mathcal{Z}_2)$, such that $\mathcal{H}_i < \mathcal{Z}_i < \mathcal{G}_i$ with $i = 1, 2$, which also satisfies the symmetry conditions listed above. The concept of maximal symmetry transition paths can also be generalized to include in addition, the specific atomic displacements that are involved in the path description. Strictly speaking, a transition path would be of maximal symmetry if the atomic displacements involved in the path cannot take place in a symmetry higher than the one being considered. In other words, a path $(\mathcal{H}_1, \mathcal{H}_2)$ would still be of maximal symmetry even in the case of the existence of a pair of intermediate subgroups $(\mathcal{Z}_1, \mathcal{Z}_2)$ fulfilling the symmetry conditions, if the atom trajectories or the lattice strains involved in the path within the symmetries $(\mathcal{H}_1, \mathcal{H}_2)$ are not compatible with the symmetries $(\mathcal{Z}_1, \mathcal{Z}_2)$. For a given set of atomic displacements linking the two end phases we expect as the most favourable trajectories those with the maximal symmetry compatible with their endpoints, and in this sense paths with very low symmetry can be of maximal symmetry in this general sense. This is for instance the case of the mechanism with symmetry $P2_1/m$ for the transformation between structure types NaCl (B1) and CsCl (B2) proposed by Stokes and Hatch [5], or the path of symmetry $P2$ proposed by Catti [17] for the transformation from structure types NaCl to *anti-litharge* in AgCl. However, most of the transition paths described or proposed in literature are in fact of maximal symmetry in the more restrictive sense represented by the first definition given above. In the following, we will only consider and use the term *transition paths of maximal symmetry* according to this restrictive definition.

The maximal symmetry transition paths, specified by the subgroups $(\mathcal{H}_1, \mathcal{H}_2)$ of highest symmetry, describe families of possible paths characterized by subgroups $(\mathcal{K}_1, \mathcal{K}_2)$, with $\mathcal{K}_i < \mathcal{H}_i < \mathcal{G}_i$ and $i = 1, 2$. They allow to classify the different possibilities for relating two structures, and by definition, every physically possible transition path must be among the set of maximal symmetry transition paths or within one of their corresponding families.

It is important to notice that the space group type of the common subgroup and the indices in $\mathcal{G}_1$ and $\mathcal{G}_2$ are not sufficient to determine if the pair $(\mathcal{H}_1, \mathcal{H}_2)$ defines a transition path of maximal symmetry. Consider for instance the $Cmc2_1$ and $Pna2_1$ transition paths in the transformation between wurtzite and NaCl structure types (see figure 1). In the case of the $Cmc2_1$ path there are three subgroups of type $Cmc2_1$ distributed in one class of conjugate subgroups in the hexagonal branch, and 6 subgroups of type $Cmc2_1$ distributed in one class of conjugate subgroups in the cubic branch. The Wyckoff splitting scheme is the same for all the subgroups in any class. The analysis of the group–subgroup graph of $Cmc2_1$ indicates that there are no intermediate subgroup that satisfies the symmetry conditions, and so, $Cmc2_1$

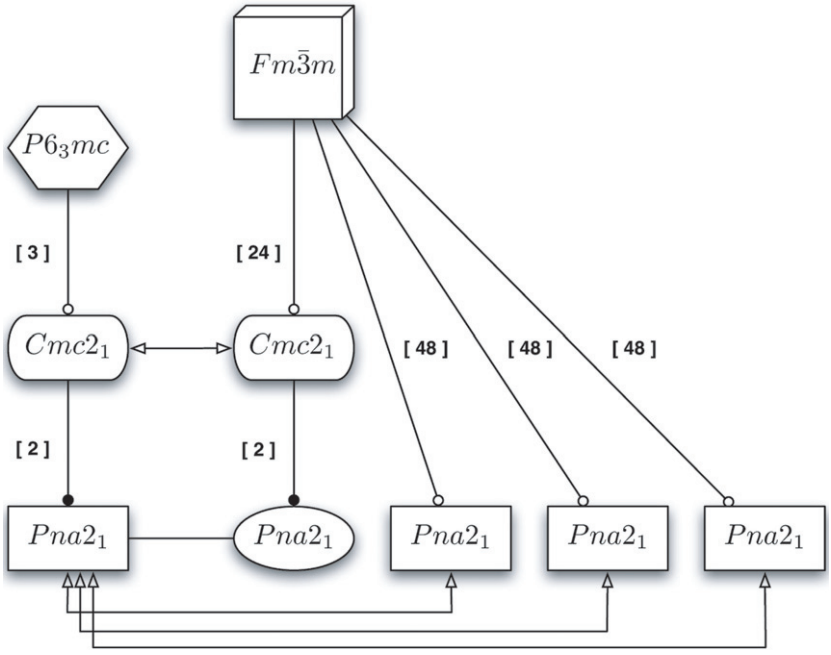

Figure 1. Symmetry relations for the wurtzite to NaCl transformation via intermediate subgroups $Cmc2_1$ and $Pna2_1$. Both $Cmc2_1$ subgroups, and $Pna2_1$ subgroups of $Fm\bar{3}m$ that are not subgroups of $Cmc2_1$, correspond to maximal symmetry transition paths.

defines a maximal symmetry transition path. In the case of the $Pna2_1$ path, the situation is somehow different. In the hexagonal branch, there are three $Pna2_1$ subgroups in one single class fulfilling $P6_3mc > Cmc2_1 > Pna2_1$. In the cubic branch, there exists 42 subgroups distributed in four classes. One of these $Pna2_1$ classes correspond to the subgroup of $Cmc2_1$, while the subgroups of the other three classes are not subgroups of $Cmc2_1$. The combinations of the three $Pna2_1$ classes of the cubic branch with the $Pna2_1$ representative of the hexagonal branch result in three additional distinct $Pna2_1$ transition paths of maximal symmetry.

2. Structural conditions on transition paths

Once a set of maximal symmetry transition paths have been determined for a certain symmetry change, as given by pairs of transformation matrices $(\boldsymbol{P}, \boldsymbol{p})_1$ and $(\boldsymbol{P}, \boldsymbol{p})_2$ for $\mathcal{G}_1 \rightarrow \mathcal{H}_1$ and $\mathcal{G}_2 \rightarrow \mathcal{H}_2$, the application of some structural conditions can help to assess their plausibility as physically relevant transition paths for a particular material. These additional structural conditions would in general constrain further the transformation matrices which define the lattice strain and the possible atomic displacements linking the two end phases.

It is reasonable to think that transformations with smaller atomic displacements and lattice strains are in general favoured with respect to other transformations which involve bigger changes. This general qualitative criterion can be translated into quantitative parameters (tolerances) or figures of merit that can be used to discard some possible paths and to classify the remaining ones. Note that, in contrast to the symmetry conditions, these additional structural conditions have to be applied separately to each particular compound and requires specific structural data of the two end phases.

We have considered two structural criteria: the magnitude of deformation of the lattice and the maximal atomic displacement that occur during the affine transformation $\mathcal{H}_1 \rightarrow \mathcal{H}_2$. The first one, restricts the arbitrariness of the rotational parts of the transformation matrices $(\boldsymbol{P}, \boldsymbol{p})_1$ and $(\boldsymbol{P}, \boldsymbol{p})_2$.

2.1. Deformation of the lattice

The assessment of the lattice strain involved in a transition path has been done in two steps. First, the mapping of the lattices of $\mathcal{H}_1$ and $\mathcal{H}_2$ has been optimized to minimize the magnitude of this strain, as measured by the so-called *metric distance* [18]. Using the freedom in the choice of the transformation matrices $(\boldsymbol{P}, \boldsymbol{p})_1$ and $(\boldsymbol{P}, \boldsymbol{p})_2$, given by the Euclidean normalizer $\mathcal{N}_{\mathcal{E}}(\mathcal{H})$, the pair of unit cells that gives the smallest deformation is selected. In a second step, a more detailed evaluation of this optimized path strain is done calculating the finite Lagrangian strain tensor. A derived scalar quantity [19], is then used as a measure of the magnitude of this strain.

The *metric distance d* is defined as follows: the metric tensor G for a unit cell a, b, c can be represented as a point h in a six-dimensional space [18]:

$$h = \begin{pmatrix} \mathbf{a}\cdot\mathbf{a} \\ \mathbf{b}\cdot\mathbf{b} \\ \mathbf{c}\cdot\mathbf{c} \\ 2\mathbf{b}\cdot\mathbf{c} \\ 2\mathbf{a}\cdot\mathbf{c} \\ 2\mathbf{a}\cdot\mathbf{b} \end{pmatrix} = \begin{pmatrix} a^2 \\ b^2 \\ c^2 \\ 2bc\cos(\alpha) \\ 2ac\cos(\beta) \\ 2ab\cos(\gamma) \end{pmatrix}. \tag{3}$$

The *metric distance d* between two unit cells is then defined as the *distance* between the corresponding two points in this six-dimensional space, and is a rough measure of the magnitude of the strain relating both cells. The finite Lagrangian strain tensor η used in the second step can be calculated in a Cartesian reference system as [20, 21]

$$\eta = \tfrac{1}{2}(e + e^{\mathrm{T}} + e^{\mathrm{T}}e) = \tfrac{1}{2}((R_1^{-1})^{\mathrm{T}} G_2 R_1^{-1} - I) \tag{4}$$

where $e = R_2 R_1^{-1} - I$, G_2 is the metric tensor for the lattice parameters of $\mathcal{H}_2$, and I is the identity matrix. The *standard root tensors* R_i provide the coordinate transformations from the conventional bases of the two unit cells to the Cartesian one. Following Schmahl [19], a convenient parameter for a quantitative evaluation of the degree of deformation of a lattice is given by:

$$\mathcal{S} = \tfrac{1}{3}\sqrt{\sum_{i=1}^{3} \eta_i^2} \tag{5}$$

where η_i are the eigenvalues of the finite Lagrangian strain tensor. In our analysis, transition paths characterized by a parameter $\mathcal{S}$ that exceeds a certain tolerance value $\mathcal{S}_{\mathrm{tol}}$ are discarded.

2.2. Atomic mappings

The second structural criterion refers to the evaluation of the atomic displacements involved in the transformation mechanism. The atomic positions of the two structures are represented in the basis of the common subgroup and the variable parameters in the Wyckoff position description indicate the relevant structural parameters (internal degrees of freedom) for the transformation. In general, there exist more than one possibility to pair the atoms between the two structures for a given common subgroup. The path is not fully defined until this atom-to-atom mapping between the two end phases is introduced. We have considered as the most

favourable mapping the one that minimizes the maximal atomic displacement required for the transformation. These estimated displacements are only qualitative, as they are calculated without taking into account the accompanying lattice strain. In addition, a tolerance value Δ_{tol} is introduced, so that transition paths with this minimized maximal distance, $\Delta_{\mathrm{max}} > \Delta_{\mathrm{tol}}$ are discarded.

With the above mentioned parameters estimating the lattice deformation and the atomic displacements, it is possible to classify the different mechanisms assessing their relevance. Smaller values for the strain and the atomic displacements would indicate a competitive mechanism.

3. Application to some reconstructive phase transitions

The above described procedure for the determination of possible transition paths of maximal symmetry have been implemented in a computer program [22], using the databases and tools provided by the *Bilbao Crystallographic Server* [23]. In the following we present the results of its application on three different types of reconstructive phase transitions, namely, the transformations between the following structure types: wurtzite to NaCl, zincblende to NaCl, and CsCl to NaCl. The assessment of the plausibility of the obtained transitions paths and the application of the tolerance limits have been necessarily done in each case for a specific material. However, one expects that for the three types of reconstructive transitions that have been studied the tolerance values are sufficiently large to include all paths that may be competitive in any material.

3.1. Wurtzite (B4) to NaCl (B1) transformation in GaN

Most of the compounds with AB stoichiometry, as for example, II–VI and III–V semiconductors with atoms in coordination 4, crystallize at normal conditions in zincblende or wurtzite structure types. One of the stable phases at high pressure is the cubic NaCl structure type, with atoms in coordination 6. In some compounds, the high pressure phase NaCl is preceded by other modifications, but there exist numerous examples of direct transformations from wurtzite to NaCl structure types [24]. Some examples of such transformations are given in materials with high technological applications as type III nitrides, AlN, GaN and InN, or the compounds of ZnO and CdSe. The structure of wurtzite crystallizes in the hexagonal space group $P6_3mc$ (186) where A and B atoms occupy Wyckoff positions $2b(\frac{1}{3}, \frac{2}{3}, z)$ with $z_{\mathrm{A}} = 0$ and $z_{\mathrm{B}} \simeq \frac{3}{8}$. In the case of the NaCl structure type, the crystal symmetry is given by the cubic space group $Fm\bar{3}m$(225) with atoms in Wyckoff positions $4a(0, 0, 0)$ and $4b(\frac{1}{2}, \frac{1}{2}, \frac{1}{2})$.

This transformation has been the object of many experimental and theoretical studies. Limpijumnong and Lambrecht [25] proposed a homogeneous orthorhombic deformation in GaN and MgO, without defining unambiguously the corresponding transition path. Sowa [26] described the transition as a deformation of a heterogeneous sphere packing via an intermediate phase with $Cmc2_1$(36) symmetry. The transition path obtained by Sowa was later identified by Perez-Mato *et al* [27] as being of maximal symmetry. By molecular dynamics techniques and DFT calculations, Shimojo [28] obtained two new transition paths, but unfortunately with insufficient information for the complete specification of the intermediate states. Sowa [29] completed one of the proposals of Shimojo, providing the complete crystallographic description of the mechanism by means of $Pna2_1$(33) symmetry.

The application of the procedure for the determination of maximal symmetry transition paths for the transformation from wurtzite to NaCl structure types for a maximum k-index of 4, results in 44 possible symmetries (see table 1). The atomic displacements and lattice strains

Table 1. Maximal symmetry transition paths for the transformation between wurtzite (B4) and NaCl (B1) structure types with a maximum k-index equal to 4. In the table, the common subgroups and their corresponding indices are given. In the last column, the number of transitions paths within the corresponding space group symmetry is specified. The total number of possible transition paths (44 distinct paths from the symmetry viewpoint) is drastically reduced when the structural conditions are applied for a specific material (see tables 2 and 3).

$\mathcal{H}$	$Z_{\mathcal{H}}$	i_1	i_1^k	i_2	i_2^k	No.
(036) $Cmc2_1$	4	3	1	24	2	1
(033) $Pna2_1$	4	6	2	48	4	3
(031) $Pmn2_1$	4	6	2	48	4	3
(026) $Pmc2_1$	4	6	2	48	4	3
(009) Cc	4	6	1	48	2	1
(008) Cm	4	6	1	48	2	1
(004) $P2_1$	2	6	1	48	2	1
(009) Cc	8	12	2	96	4	8
(008) Cm	8	12	2	96	4	4
(007) Pc	4	12	2	96	4	15
(006) Pm	4	12	2	96	4	2
(004) $P2_1$	4	12	2	96	4	2

Table 2. Maximal symmetry transition paths for the wurtzite (B4) to NaCl (B1) transformation in GaN, for a maximum k-index equal to 4, maximum allowed strain $\mathcal{S}_{\text{tol}} = 0.15$ and maximum atomic displacement $\Delta_{\text{tol}} = 2$ Å. The space group type of the common subgroup $\mathcal{H}$, the number of formula units per conventional unit cell, $Z_{\mathcal{H}}$, and the indices i_1 e i_2 of the two group–subgroup branches $\mathcal{G}_1 > \mathcal{H}_1$ and $\mathcal{G}_2 > \mathcal{H}_2$ are specified. In the last column, the transformation matrices $(\boldsymbol{P}, \boldsymbol{p})_1$ and $(\boldsymbol{P}, \boldsymbol{p})_2$, that relate the bases of the space groups of the stable phase with subgroups $\mathcal{H}_1$ and $\mathcal{H}_2$ are shown. The monoclinic axis is along b for the monoclinic space group Pc (paths numbers 5–8).

No.	$\mathcal{H}$	$Z_{\mathcal{H}}$	i	Transformation matrices $(\boldsymbol{P}, \boldsymbol{p})$
1	(036) $Cmc2_1$	4	3	$-\mathbf{a}-\mathbf{b}, \mathbf{a}-\mathbf{b}, \mathbf{c}$
			24	$-\mathbf{a}-\frac{1}{2}, -\mathbf{b}-\frac{1}{4}, \mathbf{c}$
2	(033) $Pna2_1$	4	6	$-\mathbf{a}+\mathbf{b}, -\mathbf{a}-\mathbf{b}, \mathbf{c}$
			48	$\mathbf{a}-\mathbf{b}+\frac{1}{4}, \frac{1}{2}\mathbf{a}+\frac{1}{2}\mathbf{b}-\frac{1}{2}, -\mathbf{c}$
3	(031) $Pmn2_1$	4	6	$-\mathbf{a}-\mathbf{b}+\frac{1}{4}, \mathbf{a}-\mathbf{b}-\frac{1}{4}, \mathbf{c}$
			48	$\frac{1}{2}\mathbf{a}-\frac{1}{2}\mathbf{c}+\frac{1}{8}, -\mathbf{a}-\mathbf{c}, -\mathbf{b}+\frac{1}{8}$
4	(026) $Pmc2_1$	4	6	$-\mathbf{a}-\mathbf{b}, \mathbf{a}-\mathbf{b}, \mathbf{c}$
			48	$-\frac{1}{2}\mathbf{a}+\frac{1}{2}\mathbf{b}, \mathbf{c}, \mathbf{a}+\mathbf{b}$
5	(008) Cm	4	6	$-\mathbf{a}+\mathbf{b}, -\mathbf{a}-\mathbf{b}, \mathbf{c}$
			48	$-\frac{1}{2}\mathbf{a}+\mathbf{b}+\frac{1}{2}\mathbf{c}, \frac{1}{2}\mathbf{a}+\frac{1}{2}\mathbf{c}, \frac{1}{2}\mathbf{a}+\mathbf{b}-\frac{1}{2}\mathbf{c}$
6	(007) Pc	4	12	$-2\mathbf{a}-\mathbf{b}-\mathbf{c}, \mathbf{b}+\frac{1}{4}, 2\mathbf{a}+\mathbf{b}$
			96	$-\frac{1}{2}\mathbf{a}-\mathbf{b}+\frac{1}{2}\mathbf{c}, -\frac{1}{2}\mathbf{a}-\frac{1}{2}\mathbf{c}, \mathbf{a}-\mathbf{c}$
7	(007) Pc	4	12	$-2\mathbf{a}-\mathbf{b}-\mathbf{c}, \mathbf{b}+\frac{1}{4}, 2\mathbf{a}+\mathbf{b}$
			96	$-2\mathbf{b}+\frac{3}{8}, \frac{1}{2}\mathbf{a}+\frac{1}{2}\mathbf{c}, -\frac{1}{2}\mathbf{a}+\mathbf{b}+\frac{1}{2}\mathbf{c}+\frac{3}{8}$
8	(007) Pc	4	12	$-2\mathbf{a}-\mathbf{b}-\mathbf{c}, \mathbf{b}+\frac{1}{4}, 2\mathbf{a}+\mathbf{b}$
			96	$-\mathbf{a}+\mathbf{b}-\mathbf{c}, -\frac{1}{2}\mathbf{b}-\frac{1}{2}\mathbf{c}, -\mathbf{b}+\mathbf{c}$

used have been of the structures of GaN. The experimental lattice parameters are $a = 3.1901$ Å and $c = 5.189$ Å for the wurtzite (hexagonal) [30] structure type and $a = 4.006$ Å for the NaCl

Table 3. Atomic coordinates, atomic mappings, lattice strain $\mathcal{S}$ and maximum distance $\Delta_{\max}$ of the maximal symmetry transition paths for the wurtzite (B4) to NaCl (B1) transformation in GaN, for a maximum k-index equal to 4, maximum allowed strain $\mathcal{S}_{\text{tol}} = 0.15$ and maximum atomic displacement $\Delta_{\text{tol}} = 2$ Å. The internal degrees of freedom are written in bold.

No.	$\mathcal{H}$	$\mathcal{S}$	$\Delta_{\max}$ (Å)	AT	WP	Coord. in S_1			Coord. in S_2		
1	(036) $Cmc2_1$	0.1415	0.7954	Ga	4*a*	0	$\mathbf{\frac{1}{3}}$	0	0	$\mathbf{\frac{1}{4}}$	0
				N	4*a*	0	$\mathbf{\frac{1}{3}}$	$\mathbf{\frac{3}{8}}$	0	$\mathbf{\frac{1}{4}}$	$\mathbf{\frac{1}{2}}$
2	(033) $Pna2_1$	0.0765	1.0534	Ga	4*a*	$\mathbf{\frac{1}{6}}$	$\mathbf{\frac{1}{2}}$	0	$\mathbf{\frac{1}{8}}$	$\mathbf{\frac{1}{4}}$	0
				N	4*a*	$\mathbf{\frac{1}{6}}$	$\mathbf{\frac{1}{2}}$	$\mathbf{\frac{3}{8}}$	$\mathbf{\frac{1}{8}}$	$\mathbf{\frac{1}{4}}$	$\mathbf{\frac{1}{2}}$
3	(031) $Pmn2_1$	0.0765	1.7372	Ga1	2*a*	0	$\mathbf{\frac{1}{12}}$	0	0	$\mathbf{\frac{1}{8}}$	0
				Ga2	2*a*	0	$\mathbf{\frac{3}{12}}$	$\mathbf{\frac{1}{2}}$	0	$\mathbf{\frac{5}{8}}$	**0**
				N1	2*a*	0	$\mathbf{\frac{1}{12}}$	$\mathbf{\frac{3}{8}}$	0	$\mathbf{\frac{1}{8}}$	$\mathbf{\frac{1}{2}}$
				N2	2*a*	0	$\mathbf{\frac{3}{12}}$	$\mathbf{\frac{7}{8}}$	0	$\mathbf{\frac{5}{8}}$	$\mathbf{\frac{1}{2}}$
4	(026) $Pmc2_1$	0.0923	1.9526	Ga1	2*a*	0	$\mathbf{\frac{1}{3}}$	0	0	**0**	0
				Ga2	2*b*	$\frac{1}{2}$	$\mathbf{\frac{5}{6}}$	**0**	$\frac{1}{2}$	$\mathbf{\frac{1}{2}}$	$\mathbf{\frac{1}{4}}$
				N1	2*a*	0	$\mathbf{\frac{1}{3}}$	$\mathbf{\frac{3}{8}}$	0	$\mathbf{\frac{1}{2}}$	$\mathbf{\frac{1}{2}}$
				N2	2*b*	$\frac{1}{2}$	$\mathbf{\frac{5}{6}}$	$\mathbf{\frac{3}{8}}$	$\frac{1}{2}$	**0**	$\mathbf{\frac{1}{4}}$
5	(008) Cm	0.1446	1.8417	Ga1	2*a*	$\mathbf{\frac{1}{6}}$	$\frac{1}{2}$	0	$\mathbf{\frac{1}{2}}$	$\frac{1}{2}$	0
				Ga2	2*a*	$\mathbf{\frac{5}{6}}$	$\frac{1}{2}$	$\frac{1}{2}$	$\mathbf{\frac{1}{2}}$	$\frac{1}{2}$	$\frac{1}{2}$
				N1	2*a*	$\mathbf{\frac{1}{6}}$	$\frac{1}{2}$	$\mathbf{\frac{3}{8}}$	**0**	$\frac{1}{2}$	$\mathbf{\frac{1}{4}}$
				N2	2*a*	$\mathbf{\frac{5}{6}}$	$\frac{1}{2}$	$\mathbf{\frac{7}{8}}$	**0**	$\frac{1}{2}$	$\mathbf{\frac{3}{4}}$
6	(007) Pc	0.1379	1.2182	Ga1	2*a*	0	$\mathbf{\frac{1}{4}}$	$\mathbf{\frac{1}{6}}$	0	**0**	**0**
				Ga2	2*a*	$\frac{1}{2}$	$\mathbf{\frac{1}{4}}$	$\mathbf{\frac{1}{3}}$	$\frac{1}{2}$	$\mathbf{\frac{1}{2}}$	$\mathbf{\frac{1}{2}}$
				N1	2*a*	$\mathbf{\frac{5}{8}}$	$\mathbf{\frac{1}{4}}$	**0.7916**	$\mathbf{\frac{1}{2}}$	**0**	$\mathbf{\frac{3}{4}}$
				N2	2*a*	$\mathbf{\frac{1}{8}}$	$\mathbf{\frac{1}{4}}$	**0.9583**	**0**	$\mathbf{\frac{1}{2}}$	$\mathbf{\frac{3}{4}}$
7	(007) Pc	0.0846	1.8417	Ga1	2*a*	0	$\frac{1}{4}$	$\mathbf{\frac{1}{6}}$	0	$\frac{1}{4}$	**0**
				Ga2	2*a*	$\frac{1}{2}$	$\frac{1}{4}$	$\mathbf{\frac{1}{3}}$	$\frac{1}{2}$	$\frac{1}{4}$	**0**
				N1	2*a*	$\mathbf{\frac{5}{8}}$	$\frac{1}{4}$	**0.7916**	$\mathbf{\frac{3}{4}}$	$\frac{1}{4}$	**0**
				N2	2*a*	$\mathbf{\frac{1}{8}}$	$\frac{1}{4}$	**0.9583**	$\mathbf{\frac{1}{4}}$	$\frac{1}{4}$	**0**
8	(007) Pc	0.0765	1.3801	Ga1	2*a*	0	$\mathbf{\frac{1}{4}}$	$\mathbf{\frac{1}{6}}$	0	**0**	**0**
				Ga2	2*a*	$\frac{1}{2}$	$\mathbf{\frac{1}{4}}$	$\mathbf{\frac{1}{3}}$	$\frac{1}{2}$	$\mathbf{\frac{1}{2}}$	$\mathbf{\frac{1}{4}}$
				N1	2*a*	$\mathbf{\frac{5}{8}}$	$\mathbf{\frac{1}{4}}$	**0.7916**	$\mathbf{\frac{1}{2}}$	**0**	$\mathbf{\frac{1}{2}}$
				N2	2*a*	$\mathbf{\frac{1}{8}}$	$\mathbf{\frac{1}{4}}$	**0.9583**	**0**	$\mathbf{\frac{1}{2}}$	$\mathbf{\frac{3}{4}}$

(cubic) [31] structure type. Considering $\mathcal{S}_{\text{tol}} < 0.15$ and $\Delta_{\text{tol}} < 2$ Å, we reduce the 44 possible maximal transition paths to eight transition paths with different orthorhombic and monoclinic symmetries (tables 2 and 3). In table 2, the transformation matrices $(\boldsymbol{P}, \boldsymbol{p})_1$ and $(\boldsymbol{P}, \boldsymbol{p})_2$, that relate the symmetry groups $\mathcal{G}_1 = P6_3mc(186)$ and $\mathcal{G}_2 = Fm\bar{3}m(225)$ with the intermediate common subgroups $\mathcal{H}$, are specified. Also, the indices of the corresponding group–subgroup branches i_1 and i_2, and the number of formula units per conventional unit cell $Z_{\mathcal{H}}$ are given. With the help of these transformations the unit cells of the structures in the subgroup basis are

Table 4. Maximal symmetry transition paths for the zincblende (B3) to NaCl (B1) transformation, for a maximum k-index equal to 3. The maximal common subgroups, their corresponding indices and transformation matrices are specified in the table. The transformation matrices have been optimized, when symmetry allowed, using the structural data of SiC. The rhombohedral group $R3m$ (path number 1) is described in the hexagonal basis, while the unique axis for the monoclinic space group $P2_1$ (path number 6) is along b. An additional path (path number 7) with k-index = 4 is also included (see text).

No.	$\mathcal{H}$	$Z_{\mathcal{H}}$	i	Transformation matrices $(\boldsymbol{P}, \boldsymbol{p})$
1	(160) $R3m$	3	4	$-\frac{1}{2}\mathbf{a}+\frac{1}{2}\mathbf{b}, -\frac{1}{2}\mathbf{b}+\frac{1}{2}\mathbf{c}, \mathbf{a}+\mathbf{b}+\mathbf{c}$
			8	$-\frac{1}{2}\mathbf{a}+\frac{1}{2}\mathbf{b}, -\frac{1}{2}\mathbf{b}+\frac{1}{2}\mathbf{c}, \mathbf{a}+\mathbf{b}+\mathbf{c}$
2	(044) $Imm2$	2	6	$-\frac{1}{2}\mathbf{a}+\frac{1}{2}\mathbf{c}, \frac{1}{2}\mathbf{a}+\frac{1}{2}\mathbf{c}, \mathbf{b}$
			12	$\frac{1}{2}\mathbf{a}+\frac{1}{2}\mathbf{b}, \mathbf{c}, \frac{1}{2}\mathbf{a}-\frac{1}{2}\mathbf{b}$
3	(145) $P3_2$	3	24	$-\frac{1}{2}\mathbf{a}+\frac{1}{2}\mathbf{b}, -\frac{1}{2}\mathbf{b}+\frac{1}{2}\mathbf{c}-\frac{1}{6}, \mathbf{a}+\mathbf{b}+\mathbf{c}+\frac{1}{6}$
			48	$\frac{1}{2}\mathbf{b}-\frac{1}{2}\mathbf{c}, \frac{1}{2}\mathbf{a}-\frac{1}{2}\mathbf{b}-\frac{1}{6}, -\mathbf{a}-\mathbf{b}-\mathbf{c}+\frac{1}{6}$
4	(144) $P3_1$	3	24	$-\frac{1}{2}\mathbf{a}+\frac{1}{2}\mathbf{b}-\frac{1}{6}, -\frac{1}{2}\mathbf{b}+\frac{1}{2}\mathbf{c}, \mathbf{a}+\mathbf{b}+\mathbf{c}+\frac{1}{6}$
			48	$\frac{1}{2}\mathbf{a}-\frac{1}{2}\mathbf{b}-\frac{1}{3}, \frac{1}{2}\mathbf{b}-\frac{1}{2}\mathbf{c}-\frac{1}{6}, \mathbf{a}+\mathbf{b}+\mathbf{c}+\frac{1}{2}$
5	(031) $Pmn2_1$	2	12	$-\frac{1}{2}\mathbf{a}+\frac{1}{2}\mathbf{c}+\frac{1}{8}, \frac{1}{2}\mathbf{a}+\frac{1}{2}\mathbf{c}, \mathbf{b}+\frac{1}{8}$
			24	$-\frac{1}{2}\mathbf{a}+\frac{1}{2}\mathbf{c}-\frac{1}{8}, \frac{1}{2}\mathbf{a}+\frac{1}{2}\mathbf{c}, \mathbf{b}+\frac{3}{8}$
6	(004) $P2_1$	2	24	$-\mathbf{a}-\frac{1}{4}, \mathbf{c}, \frac{1}{2}\mathbf{a}+\frac{1}{2}\mathbf{b}$
			48	$\mathbf{a}, \mathbf{b}, -\frac{1}{2}\mathbf{a}+\frac{1}{2}\mathbf{c}+\frac{1}{4}$
7	(198) $P2_13$	4	8	$\mathbf{a}+\frac{1}{2}, \mathbf{b}+\frac{1}{2}, \mathbf{c}$
			16	$\mathbf{a}+\frac{1}{2}, \mathbf{b}+\frac{1}{2}, \mathbf{c}$

defined. The resulting magnitude of the lattice strain and the optimized atomic displacements are given in table 3, where the end structures are shown in the reference frame of the subgroup. In each case, the table lists the lattice deformation as estimated by the parameter $\mathcal{S}$, and the maximum absolute distance $\Delta_{\max}$ for the mapping of the atoms with respect to the unit cell of S_1, i.e., the wurtzite structure in our case.

The transition paths with symmetries $Cmc2_1(36)$ and $Pna2_1(33)$ are equivalent to those proposed by Sowa [26, 29]. To the best of our knowledge, the rest of the paths listed in tables 2 and 3 are proposed here for the first time. The two transition paths with monoclinic symmetry $Pc(7)$ (paths number 6 and 8) are particularly interesting as their structural parameters, $\mathcal{S}$ and $\Delta_{\max}$, are similar to those of the paths proposed by Sowa.

3.2. Zincblende (B3) to NaCl (B1) transformation in SiC

Many II–VI and III–V semiconductors adopt the zincblende structure type as fundamental crystal state. The zincblende structure crystallizes in the space group $F\bar{4}3m(216)$ with atoms in $2b$ positions, $(\frac{1}{3}, \frac{2}{3}, 0)$ and $(\frac{1}{3}, \frac{2}{3}, \frac{3}{8})$. The zincblende to NaCl transformation at high pressures has been widely studied in the literature due to the number of materials with technological interest which undergo such transition. A well-known representative is SiC, a widely used material of practical importance in electronic devices, abrasives and refractants.

The first transition path proposed in the literature is based on an intermediate state with symmetry $R3m(160)$ [32]. An alternative transition path with symmetry $P2_13(198)$, was considered as clearly unfavourable [32]. Catti [2, 33, 27], based on LCAO-DFT *ab initio*

Table 5. Atomic coordinates, atomic mappings, lattice strain $\mathcal{S}$ and maximum distance Δ_{max} of the maximal symmetry transition paths for the zincblende (B3) to NaCl (B1) transformation in SiC, for a maximum k-index equal to 3, maximum lattice strain $\mathcal{S}_{tol} = 0.2$ and maximum displacement $\Delta_{tol} = 2$ Å. The internal degrees of freedom are written in bold.

No.	$\mathcal{H}$	$\mathcal{S}$	Δ_{max} (Å)	AT	WP	Coord. in S_1			Coord. in S_2		
1	(160) $R3m$	0.0406	1.7208	Si	$3a$	0	0	0	0	0	0
				C	$3a$	0	0	$\mathbf{\frac{1}{4}}$	0	0	$\mathbf{\frac{1}{2}}$
2	(044) $Imm2$	0.2335	0.9935	Si	$2a$	0	0	0	0	0	0
				C	$2b$	0	$\frac{1}{2}$	$\mathbf{\frac{1}{4}}$	0	$\frac{1}{2}$	**0**
3	(145) $P3_2$	0.0406	1.0983	Si	$3a$	**0**	$\mathbf{\frac{2}{3}}$	0	$\mathbf{\frac{1}{3}}$	**0**	0
				C	$3a$	0	$\mathbf{\frac{2}{3}}$	$\mathbf{\frac{1}{4}}$	0	$\mathbf{\frac{1}{3}}$	$\mathbf{\frac{1}{6}}$
4	(144) $P3_1$	0.0406	1.0983	Si	$3a$	$\frac{2}{3}$	$\mathbf{\frac{2}{3}}$	0	$\frac{2}{3}$	**0**	0
				C	$3a$	$\mathbf{\frac{2}{3}}$	$\mathbf{\frac{2}{3}}$	$\mathbf{\frac{1}{4}}$	$\mathbf{\frac{1}{3}}$	$\mathbf{\frac{1}{3}}$	$\mathbf{\frac{1}{6}}$
5	(031) $Pmn2_1$	0.0406	1.4050	Si	$2a$	**0**	$\frac{3}{4}$	0	$\mathbf{\frac{1}{2}}$	$\frac{3}{4}$	0
				C	$2a$	$\frac{1}{2}$	$\frac{3}{4}$	$\mathbf{\frac{3}{4}}$	$\frac{1}{2}$	$\frac{3}{4}$	$\mathbf{\frac{1}{2}}$
6	(004) $P2_1$	0.0406	1.4050	Si	$2a$	$\frac{3}{4}$	0	**0**	$\frac{3}{4}$	0	$\mathbf{\frac{1}{2}}$
				C	$2a$	$\frac{3}{4}$	$\mathbf{\frac{1}{4}}$	$\frac{1}{2}$	$\frac{3}{4}$	$\mathbf{\frac{1}{2}}$	$\frac{1}{2}$
7	(198) $P2_13$	0.0406	1.7208	Si	$4a$	0	0	0	0	0	0
				C	$4a$	$\mathbf{\frac{1}{4}}$	$\mathbf{\frac{1}{4}}$	$\mathbf{\frac{1}{4}}$	$\mathbf{\frac{1}{2}}$	$\mathbf{\frac{1}{2}}$	$\mathbf{\frac{1}{2}}$

calculations, proposed an alternative orthorhombic mechanism of $Imm2(44)$ symmetry that appeared to be energetically more favourable than the rhombohedral one, in the case of SiC and ZnS. The same orthorhombic mechanism was confirmed by Sowa [34] who later proposed a third one [35] based on a trigonal intermediate symmetry $P3_2(145)$. Recently, Stokes and Hatch [11] determined systematically the transition paths for the zincblende to NaCl transformation in SiC obtaining a set of eight mechanisms with an enthalpy barrier of a similar order of magnitude. Apart from the previously proposed mechanisms, the authors added new paths with monoclinic and triclinic symmetries $Cc(9)$ and $P1(1)$.

The maximal symmetry transition paths for the zincblende (B3) to NaCl (B1) transformation are listed in tables 4, and 5, for a maximum k-index equal to 3. The number of paths is not reduced after the application of the structural conditions for the data of SiC with the tolerance values of lattice strain $\mathcal{S}_{tol} = 0.2$, and maximum displacements $\Delta_{tol} = 2$ Å. The lattice parameters are $a = 3.974$ Å, for the zincblende structure, and $a = 3.684$ Å for the NaCl structure type [36]. A set of six maximal symmetry transition paths have been obtained. We have added another well known path (case 7) that results when k-index is increased to 4. The information contained in the tables is analogous to the data presented in the tables 2 and 3 and for the wurtzite to NaCl case.

The first path of the list with $R3m(160)$ symmetry corresponds to that proposed by Blanco [32], the second one with $Imm2(44)$ symmetry corresponds to Catti's solution [2] and the third path, with symmetry $P3_2(145)$, to the mechanism studied by Sowa [35]. The fourth path involves an intermediate subgroup $P3_1(144)$, physically equivalent to $P3_2(145)$, with the same $\mathcal{S}$ and Δ_{max} parameters. With a maximum k-index equal to 4, the proposed $P2_13(198)$ is also obtained. Stokes and Hatch [11] obtained the maximal symmetry transition paths 1, 2, 3 and 7 listed in table 5. They proposed, however, additional ones: (i) one with intermediate symmetry $Cc(9)$ and indices 24 and 48, (ii) two with $Cc(9)$ symmetry and indices 48 and 96,

Table 6. Maximal symmetry common subgroups for the NaCl (B1) to CsCl (B2) transformation for a k-index equal to 2. The maximal common subgroups, their corresponding indices and transformation matrices are specified. The transformation matrices have been optimized, when symmetry allowed, using the structural data of NaCl. The rhombohedral space group $R\bar{3}m$ (case 1) is described with respect to the hexagonal basis. In the monoclinic cases, the monoclinic axis is along b.

No.	$\mathcal{H}$	$Z_{\mathcal{H}}$	i	Transformation matrices $(\boldsymbol{P}, \boldsymbol{p})$
1	(166) $R\bar{3}m$	3	4	$-\mathbf{a}+\mathbf{b}, -\mathbf{b}-\mathbf{c}, -\mathbf{a}-\mathbf{b}+\mathbf{c}$
			4	$-\frac{1}{2}\mathbf{a}+\frac{1}{2}\mathbf{b}, -\frac{1}{2}\mathbf{b}+\frac{1}{2}\mathbf{c}, \mathbf{a}+\mathbf{b}+\mathbf{c}$
2	(059) $Pmmn$	2	12	$-\mathbf{a}+\mathbf{c}, \mathbf{a}+\mathbf{c}, \mathbf{b}+\frac{1}{2}$
			12	$\frac{1}{2}\mathbf{a}+\frac{1}{2}\mathbf{b}+\frac{1}{4}, \mathbf{c}, \frac{1}{2}\mathbf{a}-\frac{1}{2}\mathbf{b}+\frac{1}{4}$
3	(036) $Cmc2_1$	4	24	$-\mathbf{a}+\mathbf{c}, \mathbf{a}+\mathbf{c}, \mathbf{2b}$
			24	$-\mathbf{a}, -\mathbf{b}-\frac{1}{4}, \mathbf{c}$
4	(031) $Pmn2_1$	2	24	$-\mathbf{a}+\mathbf{b}, \mathbf{c}, \mathbf{a}+\mathbf{b}$
			24	$-\frac{1}{2}\mathbf{a}+\frac{1}{2}\mathbf{b}, \mathbf{c}, \frac{1}{2}\mathbf{a}+\frac{1}{2}\mathbf{b}+\frac{1}{4}$
5	(008) Cm	2	24	$-\mathbf{a}+\mathbf{c}, \mathbf{a}+\mathbf{c}, \mathbf{b}$
			24	$\mathbf{a}, \mathbf{c}, -\frac{1}{2}\mathbf{a}-\frac{1}{2}\mathbf{b}$
6	(007) Pc	2	48	$-\mathbf{2a}+\mathbf{b}, \mathbf{c}, \mathbf{2a}$
			48	$-\mathbf{b}+\frac{1}{8}, \frac{1}{2}\mathbf{a}+\frac{1}{2}\mathbf{c}, -\frac{1}{2}\mathbf{a}+\mathbf{b}+\frac{1}{2}\mathbf{c}+\frac{1}{8}$
7	(007) Pc	2	48	$\mathbf{a}+\mathbf{b}, \mathbf{c}, -\mathbf{2b}$
			48	$-\frac{1}{2}\mathbf{a}+\frac{1}{2}\mathbf{b}, \mathbf{c}, \mathbf{a}+\frac{1}{4}$
8	(005) $C2$	4	48	$\mathbf{2a}+\frac{1}{2}, \mathbf{2b}, -\mathbf{a}+\mathbf{c}$
			48	$-\mathbf{a}+\frac{1}{4}, -\mathbf{c}-\frac{1}{4}, \mathbf{a}-\mathbf{b}$

and (iii) two other paths with $P1(1)$ symmetry and indices 96 and 192. The last two cases have not been considered here because they imply a larger k-index. The first case, $Cc(9)$ with indices 24 and 48, is obtained as a transition path by our calculations but it is not a maximal symmetry transition path, being a subgroup of $Imm2$. It is however of maximal symmetry in the more extended sense discussed above. The new proposals, $Pmn2_1(31)$ and $P2_1(4)$, obtained here present interesting and competitive values for the strain $\mathcal{S}$ and the maximum atomic displacement $\Delta_{\max}$, when compared with the values corresponding to the previously proposed mechanisms.

3.3. NaCl (B1) to CsCl (B2) transformation in NaCl

The phase transition between the NaCl (B1) and CsCl (B2) structure types is a classical example of reconstructive transformation at high pressures. It occurs in numerous alkali halides such as NaCl, KCl, RbCl, NaBr, and alkaline earth oxides as CaO, SrO, BaO. The inverse transition is given in CsCl at high temperatures. The caesium chloride structure type crystallizes in space group $Pm\bar{3}m(221)$ with atoms in positions $1a(0, 0, 0)$ and $1b(\frac{1}{2}, \frac{1}{2}, \frac{1}{2})$ positions. The transition is accompanied of a change in the coordination number from 6 to 8. This transition has been widely studied in the literature and three main mechanisms have been proposed. The first of them is known as Buerger mechanism [37], and it is based on a rhombohedral intermediate state $R\bar{3}m$ (166). It consists on a contraction along the cubic direction [111], and a simultaneous expansion in the perpendicular direction. A different path was proposed by Watanabe *et al*, on the basis of the observations of the temperature driven transition in CsCl. This second

Table 7. Atomic coordinates, atomic mappings and maximum strain $\mathcal{S}$ and distance Δ_{max} of the maximal symmetry transition paths for the NaCl (B1) to CsCl (B2) transformation in NaCl, for a maximum k-index equal to 2, maximum lattice strain $\mathcal{S}_{tol} = 0.5$ and maximum displacement $\Delta_{tol} = 2.5$ Å. The internal degrees of freedom are written in bold.

No.	$\mathcal{H}$	$\mathcal{S}$	Δ_{max} (Å)	AT.	WP	Coord. in S_1			Coord. in S_2		
1	(166) $R\bar{3}m$	0.2845	0	Cl	3*b*	0	0	$\frac{1}{2}$	0	0	$\frac{1}{2}$
				Na	3*a*	0	0	0	0	0	0
2	(059) $Pmmn$	0.0942	0.7450	Cl	2*b*	$\frac{3}{4}$	$\frac{1}{4}$	$\mathbf{\frac{1}{2}}$	$\frac{3}{4}$	$\frac{1}{4}$	$\mathbf{\frac{3}{4}}$
				Na	2*a*	$\frac{3}{4}$	$\frac{3}{4}$	$\mathbf{0}$	$\frac{3}{4}$	$\frac{3}{4}$	$\mathbf{\frac{3}{4}}$
3	(036) $Cmc2_1$	0.0942	1.8249	Cl	4*a*	0	$\mathbf{\frac{1}{2}}$	$\mathbf{\frac{1}{4}}$	0	$\mathbf{\frac{3}{4}}$	$\mathbf{\frac{1}{2}}$
				Na	4*a*	0	$\mathbf{0}$	0	0	$\mathbf{\frac{3}{4}}$	0
4	(031) $Pmn2_1$	0.2845	2.2350	Cl	2*a*	0	$\mathbf{\frac{1}{2}}$	$\mathbf{\frac{1}{2}}$	0	$\mathbf{\frac{1}{4}}$	0
				Na	2*a*	0	$\mathbf{0}$	0	0	$\mathbf{\frac{3}{4}}$	0
5	(008) Cm	0.2383	1.5	Cl	2*a*	0	$\frac{1}{2}$	$\mathbf{\frac{1}{2}}$	0	$\frac{1}{2}$	$\mathbf{0}$
				Na	2*a*	0	0	0	0	0	0
6	(007) Pc	0.1726	1.6659	Cl	2*a*	$\frac{1}{2}$	$\mathbf{\frac{1}{2}}$	$\mathbf{\frac{3}{4}}$	$\frac{1}{2}$	$\mathbf{\frac{3}{4}}$	$\mathbf{0}$
				Na	2*a*	0	$\mathbf{0}$	0	0	$\mathbf{\frac{3}{4}}$	0
7	(007) Pc	0.3236	2.2350	Cl	2*a*	$\mathbf{\frac{1}{2}}$	$\mathbf{\frac{1}{2}}$	0	$\mathbf{0}$	$\mathbf{\frac{1}{4}}$	0
				Na	2*a*	0	$\mathbf{0}$	0	0	$\mathbf{\frac{3}{4}}$	0
8	(005) $C2$	0.4210	1.8249	Cl	4*c*	$\mathbf{\frac{1}{4}}$	$\mathbf{\frac{1}{4}}$	$\mathbf{\frac{1}{2}}$	$\mathbf{0}$	$\mathbf{\frac{1}{2}}$	$\mathbf{\frac{1}{4}}$
				Na	4*c*	$\mathbf{\frac{1}{4}}$	0	$\mathbf{0}$	$\mathbf{0}$	0	$\mathbf{\frac{3}{4}}$

mechanism is similar to one of the geometrical models suggested by Hyde and O'Keefe [38] which implies an interplanar movement and anti-parallel displacements of the atoms of the adjacent NaCl layers (100). A modified Buerger-type path has been presented by Stokes and Hatch [5, 10], which involves a monoclinic $P2_1/m$ (11) symmetry for the intermediate state. Catti [39, 3] has shown that for the $P2_1/m$ path in CaO, the crystal passes through a metastable structure of type TlI (B33), with symmetry $Cmcm$ (63) and $Z = 4$ formula units. On the other hand, Toledano [7] proposes a two-step mechanism through a B33 structure type, motivated by the experimental observation of the B33 phase in PbS.

The maximal symmetry transition paths for the NaCl (B1) to CsCl (B2) transformation are listed in tables 6, and 7, for a maximum k-index equal to 2. The total number of paths is not reduced after the application of the structural conditions for the data of NaCl ($\mathcal{S}_{tol} = 0.5$ and $\Delta_{tol} = 2.5$ Å). The lattice parameters used in the calculation are $a = 4.84$ Å, for the NaCl structure type, and $a = 2.98$ Å for the CsCl structure type according to [5]. Among the eight paths obtained, both Buerger and Watanabe mechanisms can be easily recognized, being the first and second in table 7. It is interesting to compare the remaining paths to those obtained by Stokes and Hatch [5] using a different approach. Apart from the Buerger and Watanabe paths, their work includes 10 additional paths, and only one of them can be found in our list (path number 3). This is easily explained by the different criteria applied in our search: two of the transition paths with symmetry $Cc(9)$ in [5], are excluded here as they do not fulfil the maximal symmetry criterion, while the remaining ones correspond to higher k-indices. On the other hand, the reason why paths from 4 to 8 in tables 6 and 7 were not obtained or had been discarded in [5] is not clear.

4. Conclusions

We have developed a general systematic procedure for the determination of the possible transition paths for a phase transition with no group–subgroup relation between their phases, which has been implemented in a computer program. The method is based on certain symmetry and structural criteria. It is assumed that a transition path involves a hypothetical intermediate configuration whose symmetry is given by a single common subgroup of the space groups of the two stable phases. Additional symmetry constraints follow from the occupied atomic positions. The introduction of the so-called maximal symmetry transition paths results in a convenient classification scheme. The applied symmetry conditions have general validity as they do not depend on the specific structures but just on the structure types of the two end phases. An evaluation of the plausibility of the transitions paths derived from the symmetry conditions is achieved by an additional analysis of the lattice strains and atomic displacements involved in the transition path for a specific typical material. Here, we present the results obtained for three types of reconstructive phase transitions: wurtzite to rocksalt, zincblende to rocksalt and rocksalt to caesium chloride. In the three cases, apart from the transition paths that had been previously proposed, new possible transition paths of maximal symmetry have been determined, which can be of relevance in the transformations of some specific structures.

Acknowledgments

This work has been supported by UPV/EHU (Project 00063.310-13564) and Ministerio de Ciencia y Tecnologia (MAT2005-05216).

References

[1] Zahn D and Leoni S 2004 *Phys. Rev. Lett.* **92** 250201
[2] Catti M 2001 *Phys. Rev. Lett.* **87** 035504
[3] Catti M 2004 *J. Phys.: Condens. Matter* **16** 3909–21
[4] Christy A G 1993 *Acta Crystallogr.* B **49** 987–96
[5] Stokes H T and Hatch D M 2002 *Phys. Rev.* B **65** 144114
[6] Toledano P and Dmitriev V 1996 *Reconstructive Phase Transitions* (Singapore: World Scientific)
[7] Toledano P, Knorr K, Ehm L and Depmeier W 2003 *Phys. Rev.* B **67** 144106
[8] Cahn J 1977 *Acta Metall.* **25** 721–4
[9] Sowa H 2000 *Acta Crystallogr.* A **56** 288–99
[10] Stokes H T, Hatch D M, Dong J J and Lewis J P 2004 *Phys. Rev.* B **69** 174111
[11] Hatch D M, Stokes H T, Dong J J, Gunter J, Wang H and Lewis J P 2005 *Phys. Rev.* B **71** 184109
[12] Hermann C 1929 *Z. Kristallogr.* **69** 533–55
[13] Wondratschek H 1993 *Miner. Petrol.* **48** 87–96
[14] Wondratschek H, Müller U, Aroyo M I and Sens I 1995 *Z. Kristallogr.* **210** 567–73
[15] Mailhiot C and McMahan A K 1991 *Phys. Rev.* B **44** 11578–91
[16] Koch E and Fischer W 1975 *Acta Crystallogr.* A **31** 88–95
[17] Catti M 2005 *Phys. Rev.* B **72** 064105
[18] Andrews L C and Bernstein H J 1988 *Acta Crystallogr.* A **44** 1009–18
[19] Schmahl W W 1990 *Z. Kristallogr.* **191** 23–38
[20] Schlenker J L, Gibbs G V and Boisen M B Jr 1978 *Acta Crystallogr.* A **34** 52–4
[21] Catti M 1985 *Acta Crystallogr.* A **41** 494–500
[22] Capillas C 2006 Métodos de la cristalografía computacional en el análisis de transiciones de fase estructurales *PhD Thesis* Universidad del País Vasco
[23] Aroyo M I, Perez-Mato J M, Capillas C, Kroumova E, Ivantchev S, Madariaga G, Kirov A and Wondratschek H 2006 *Z. Kristallogr.* **221** 15–27 http://www.cryst.ehu.es
[24] Mujica A, Rubio A, Muñoz A and Needs R J 2003 *Rev. Mod. Phys.* **75** 863–912
[25] Limpijumnong S and Lambrecht W R L 2001 *Phys. Rev. Lett.* **86** 91–4

[26] Sowa H 2001 *Acta Crystallogr.* A **57** 176–82
[27] Perez-Mato J M, Aroyo M I, Capillas C, Blaha P and Schwarz K 2003 *Phys. Rev. Lett.* **90** 049603
[28] Shimojo F, Kodiyalam S, Ebbsjo I, Kalia R K, Nakano A and Vashishta P 2004 *Phys. Rev.* B **70** 184111
[29] Sowa H 2005 *Acta Crystallogr.* A **61** 325–30
[30] Schultz H and Thiemann K H 1977 *Solid State Commun.* **23** 815–9
[31] Xia H, Xia Q and Ruoff A L 1993 *Phys. Rev.* B **47** 12925
[32] Blanco M A, Recio J M, Costales A and Pandey R 2000 *Phys. Rev.* B **62** R10599–602
[33] Catti M 2002 *Phys. Rev.* B **65** 224115
[34] Sowa H 2000 *Z. Kristallogr.* **215** 335–42
[35] Sowa H 2003 *Acta Crystallogr.* A **59** 266–72
[36] Yoshida M, Onodera A, Ueno M, Takemura K and Shimomura O 1993 *Phys. Rev.* B **48** 10587
[37] Buerger J M 1951 *Phase Transformations in Solids* (New York: Wiley)
[38] Hyde B G and O'Keefe M 1973 *Phase Transitions* (Oxford: Pergamon)
[39] Catti M 2003 *Phys. Rev.* B **68** 100101